Title
PSEUDOPOTENTIAL CALCULATION OF THE OPTICAL CONSTANTS OF NaCl AND KC1

Authors
Fong, C.Y.
Cohen, Marvin L.

Publication Date
1969-02-01

Submitted to Physical Review

UCRL-18356 Rev.
c.2 upl.

PSEUDOPOTENTIAL CALCULATION OF THE OPTICAL CONSTANTS OF NaCl AND KCl

C. Y. Fong and Marvin L. Cohen

February 1969

AEC Contract No. W-7405-eng-48

LAWRENCE RADIATION LABORATORY
UNIVERSITY of CALIFORNIA BERKELEY

UCRL-18356 Rev.
c.2 upl.

DISCLAIMER

UCRL-18356 Rev.

PSEUDOPOTENTIAL CALCULATION OF THE OPTICAL CONSTANTS OF NaCl AND KCl*

C. Y. Fong+

and

Marvin L. Cohen

Inorganic Materials Research Division, Lawrence Radiation Laboratory,
Department of Physics, University of California,
Berkeley, California

ABSTRACT

The electronic band structure and optical constants of NaCl and KCl are calculated using the Empirical Pseudopotential Method (EPM). The NaCl band structure was calculated using the standard EPM; however, for KCl we have added a nonlocal d-wave potential similar to that used by Falicov and Lee for potassium. The prominent structure in the measured optical spectrum of these crystals is identified.

*Supported in part by the National Science Foundation.

+Present address, Department of Physics, University of California, Davis, California 95616

I. Introduction

The ultraviolet optical properties of the alkali-halides have been studied extensively by absorption measurements[1] and reflectivity measurements[2] for photon energy from 5-12 eV at several temperatures. Recently, the reflectivities of NaCl and KCl have been measured by Roessler and Walker[3] over a wide range of photon energy (5-28 eV), and an accurate $\varepsilon_2(\omega)$ has been obtained using the Kramers-Kronig relation. In the present work, we attempt to explain the origin of the optical structure in this data by calculating the electronic energy band structure and optical constants of NaCl and KCl using the Empirical Pseudopotential Method (EPM).

Theoretical calculations of the electronic band structure of NaCl was first done by Shockley;[4] the results provide the valence bands only. Two other calculations on NaCl were reported by Tibbs[5] and Casella.[6] Tibbs' calculation gives only approximate results and Cassella's calculation provides only the valence bands. We have reported briefly on the results of our band structure and $\varepsilon_2(\omega)$ calculations using the EPM for NaCl.[7] In the present work we will give a complete critical point analysis of the band structure and attempt to give a detailed analysis of the structure in the optical spectrum.

For KCl, several calculations exist in the literature. Howland[8] calculated the valence bands, and Oyama and Miyakawa[9] calculated the conduction bands by the OPW method. DeCicco[10] used the APW method to calculate the entire band structure of KCl, however; his results appear to give only fair agreement with experiment, e.g. the calculated fundamental gap at Γ is 6.3 eV, whereas, experimentally, it is 8.69 eV. In

the present work, we have again used the EPM to explore the electronic structure of KCl. Our results should be considered to be preliminary, primarily for the following two reasons. First, we have directed our attention to the low energy regions ($\hbar\omega \leq 13$ eV) of the spectrum. Second, we add an $\ell = 2$ nonlocal pseudopotential term in order to treat the d-like conduction band states on a different footing than the s and p-like states, and to obtain convergence of 0.1 eV for the eigenvalues requires a matrix size of the order of 65 x 65. Highly accurate eigenvalues are therefore difficult to obtain, and this limits us to a great extent.

The paper is arranged as follows: In Sec. II we give an interband critical point analysis of the $\varepsilon_2(\omega)$ for NaCl. The $\varepsilon_2(\omega)$ with constant matrix elements is also given and a comparison of the conduction band density of states with the photoabsorption measurements[11] is included. In Sec. III we discuss the pseudopotential Hamiltonian with an $\ell = 2$ nonlocal pseudopotential, the choice of the form factors, the band structure, and $\varepsilon_2(\omega)$ for KCl. In Sec. IV we compare the results for NaCl and KCl.

II. Critical Point Analysis for NaCl

We have previously described[7] the method for obtaining the pseudopotential form factors for NaCl and the identification of the prominent structure in $\varepsilon_2(\omega)$. To give a more complete analysis, we give here the interband cp analysis and the $\varepsilon_2(\omega)$ with constant matrix elements (Fig. 3) for NaCl. To facilitate the discussion, we reproduce the figures for the band structure (with a few corrections for the labels of the high energy bands) and the $\varepsilon_2(\omega)$ with matrix elements computed from the pseudowavefunctions. These are given in Figs. 1 and 2. The

main features of the band structure, the exciton structure and comparisons with MgO have been discussed previously.

The fundamental gap $\Gamma_{15} \rightarrow \Gamma_1$ was adjusted to 8.97 eV to agree with the gap determined experimentally. It has M_0 symmetry as shown in the energy contour diagrams (Figs. 4, 7, 10). The next structure arises from transitions along the [111] direction, i.e. an M_0 cp at 9.86 eV arising from $L_3 \rightarrow L_2'$ transitions and an M_2 cp at 10.29 eV coming from $\Lambda_3 \rightarrow \Lambda_1$ transitions, (Figs. 4 and 7). We think it is this M_2 type singularity which causes the different shape of the corresponding peaks for NaCl and MgO. Experimentally, NaCl has a round smeared out peak, whereas MgO has a sharp peak. Differential reflectance measurements, near this energy region would be very helpful to determine the characteristics of this structure. The magnitude of this structure differs greatly between experiment and theory as it does in MgO,[12] GaAs[13] and other zincblende compounds,[14] and it is masked by the prominent X-Δ-Σ peak around 11 eV.

The largest interband peak of NaCl in the optical spectrum comes from transitions along Δ and Σ (see Table I, Figs. 2, 4 and 7); this is also found in the diamond and zincblende structure and in MgO. The M_1 singularity at $\Delta_5 \rightarrow \Delta_1$ is at 11.07 eV and the M_2 cp of $\Sigma_4 \rightarrow \Sigma_1$ is at 11.32 eV. The resultant peak is at 11.1 eV. The magnitude of this peak is strengthened by a large region in the k-space having this energy difference (Fig. 4, 5, 7, 8 and 10).

Because of the lowering of the upper conduction bands in NaCl the wide dip in $\epsilon_2(\omega)$ around 14.5 eV in MgO is absent in the corresponding 11-12 eV region in NaCl; however, there are quite a few weak cp's arising from Δ and Σ transitions (Table I, Figs. 4, 5, 7, 8, 10, 11) in this energy region.

The peak at 12.25 eV is the most distinct structure in $\varepsilon_2(\omega)$ for NaCl which is different from MgO.[12] The matrix elements for the individual interband transitions show the dominant contribution arising from an M_1 type singularity from $L_3 \rightarrow L_3'$ ($4 \rightarrow 6$ and $3 \rightarrow 6$) transitions and the M_0 type cp at L for $4 \rightarrow 7$, $3 \rightarrow 7$ transitions (Figs. 5, 6, 8 and 9). The energy contours for 12.25 eV shown in Figs. 5 and 8 illustrate the contributions to the background of the peak. The region with an M_2 cp from $\Lambda_1 \rightarrow \Lambda_1$ ($2 \rightarrow 6$) transitions at 12.61 eV also contributes (Fig. 11).

The next structure in the calculated ε_2 is at 13 eV; it is 0.3 eV lower than the corresponding structure in the experimental curve (see Fig. 2). We expect some discrepancy at high energy since our pseudopotential is taken to be energy independent. The peak starts with an M_0 cp arising from $\Gamma_{15} \rightarrow \Gamma_{25}'$ with energy 12.67 eV. The cp's in this region are quite complicated. A strong M_1 cp from $\Delta_5 \rightarrow \Delta_2'$ at 12.77 eV (Fig. 5) follows the Γ transitions. Together these form a weak peak at 12.7 eV. Another strong contribution comes from $\Lambda_3 \rightarrow \Lambda_3$ ($3 \rightarrow 7$) transitions (Fig. 9) causing the peak at 13 eV. As in the case of MgO, a large volume of the Brillouin zone contributes in this energy range (Figs. 6, 8, 9, 11, 12). The resulting structure resembles the twin peak structure in MgO; it is not clearly shown in the $\varepsilon_2(\omega)$ (Fig. 2) because the dispersion in energy as a function of wavevector for these bands is less than it is in MgO. The round peak in the experimental curve does not resolve the fine structure very well. The cp's with energy higher than 13.6 eV are listed in Table I, but they are not expected to be accurately determined because of the expected energy dependence of the pseudopotential for the higher energy bands. The theoretical and experimental ε_2 both drop as a function of energy in this energy range.

We have also calculated the density of states of the conduction bands. The results are plotted in Fig. 13 and can be used to explain the structure in the recent photoabsorption measurement on NaCl by Haensel et al.[11] These authors used the synchrotron radiation to excite the inner core states (L_{II}, L_{III}) of Na^+ causing transitions from these states to the conduction bands. The structure in the measured absorption coefficient curve must correlate with the density of states of the conduction bands. We have treated the calculated density of states of NaCl as being proportional to the absorption coefficient with constant dipole matrix elements. The peaks A and B in the experimental results are identified as the exciton excitations. The energy difference of peaks C and B is about 1 eV. If we take the binding energy of the n = 1 exciton for NaCl to be 1.2 eV, the difference in energy between the n = 2 and n = 1 exciton states is 0.9 eV. Thus we can assign tentatively the peak C in the experimental result to n = 2 exciton excitation. However, we have not included the exciton effects in our calculation; and therefore these three peaks do not have the corresponding structure in Fig. 13. The peaks in the calculated density of states curve are labeled by D, E, F, G and H; (we have calculated the conduction band density of states up to higher energies than $\varepsilon_2(\omega)$) these peaks correspond to the labeling in Ref. 11 for NaCl. The higher energy peaks, i.e. F, G and H have lower energy values than the measured values; the difference is of the order of 1 eV. As we mentioned earlier, the 13 eV peak in the uv data, which corresponds to the 12.6 eV region in the calculated density of states curve, is 0.3 eV lower in the theoretical ε_2 than the one obtained by measurement. We expect that the discrepancies in the energy values

for the higher energy peaks are of the order of 1 eV. One may point out that the structure in the region of the theoretical density of states curve around 12.6 eV corresponds to a dip in the experimental results. However, we find that the region in the BZ which contributes to this energy is near Λ_3 and L_3' (6th band); the corresponding wavefunctions have p-character. It is easy to show that the transitions from the inner p-core states to the p-like Bloch states are forbidden. The exact matrix element of the dipole transition will be decreased because one has to project out from the Bloch wavefunction that part of the wavefunction with p-characteristics. So the calculated results in Fig. 13 agree well with the experiment on photoabsorption.

III. KCl

A. Pseudopotential Hamiltonian with $\ell = 2$ Nonlocal Term

KCl has the same crystal structure as NaCl; the method described for NaCl[7] for the local part of the pseudopotential also applies to this case. We start with a set of symmetric form factors which are scaled from an average of the form factors for sodium chloride[7] and germanium.[15] The antisymmetric form factors are scaled from MgO.[12] By merely adjusting these five parameters, we cannot reach the identified energy for the $\Gamma_{15} \rightarrow \Gamma_{25}'$ transitions, and the best resulting spectrum for the above model looks very much like the one for NaCl. However, experimentally, the two spectra are completely different. We, therefore, have added a nonlocal pseudopotential for the following reason: The valence electrons in KCl consist of the (4s) electron of the K atom and the $(3s)^2(3p)^5$ electrons of the Cl atom, and the unfilled 3d states for the K^+ ion have lower energies with respect to the vacant (4s)

level than in the case of NaCl. In fact, in NaCl, the unfilled 3d states have higher energies than the vacant (3s) level for the Na^+ ion. In addition, the core states of KCl have mainly s and p character; so the approximation that complete cancellation for the s and p valence electrons from the core states in the local pseudopotential model should be reasonable. However, for the d-like conduction electrons which in KCl are more important for the low energy spectrum, the cancellation from the core will not be complete, and these bands cannot be treated on an equal footing with the s and p bands. Thus we add a nonlocal pseudopotential term for $\ell = 2$.

The pseudopotential Hamiltonian has the following form:

$$\mathcal{H} = -\frac{\hbar^2}{2m}\nabla^2 + V(\underline{r}) + V_{NL}(\underline{r}) \qquad (1)$$

where the first two terms on the right hand side are the kinetic energy and the local pseudopotential; while V_{NL} is the nonlocal pseudopotential term. The local pseudopotential has been discussed in Refs. 7 and 12; we shall now discuss V_{NL}.

We know from studies of the atomic energy levels that the energy of the d-state will be closer to the $(3p)^6$ core state in the K^+ ion than the $(2p)^6$ core states in the Cl^- ion. The effect of the core contribution to the nonlocal pseudopotential is expected to be primarily from the K^+ ion.

The form of the d-like nonlocal pseudopotential is[16]

$$V_{NL} = \sum_{\underline{R}_j} V_2 (\underline{r} - \underline{R}_j) P_2^{\ell} P_2^{r} \qquad (2)$$

where $\underline{R}_j$ is the lattice vector, and $\underline{r}$ is measured from the center of the K^+ ion. P_2^{ℓ} is a projection operator; it acts on the left of the wave function when the matrix elements of V_{NL} are taken and projects out $\ell = 2$ component only. P_2^{r} is the same kind of operator but it acts on the right, and

$$V_2(\underline{r} - \underline{R}_j) = A_2 \qquad \text{for } |\underline{r} - \underline{R}_j| \leq R_s$$

$$= 0 \qquad \text{for } |\underline{r} - \underline{R}_j| > R_s \tag{3}$$

A_2 is treated as disposable parameter and is the depth of the square-well potential. R_s is the radius of the well; it is determined from the potassium ion[16,17] and is not treated as a parameter.

The matrix elements of V_{NL} are evaluated over plane wave states with energy less than E_1. We have neglected the matrix elements for those plane waves with energies between E_1 and E_2. The resultant matrix elements of the potential energy are the sum of the matrix elements for the local pseudopotential and the $\ell = 2$ nonlocal pseudopotential. When the convergence of the few important energy gaps at the symmetry points, such as Γ, X, and L, are tested, we find that in order to keep the variation of the energy gaps within 0.1 eV, we must have E_1 and E_2 equal to 16.1 and 38.1 respectively. The size of the matrix is of the order of 65 x 65.

B. Results and Discussions

The numerical values of the form factors are given in Table II; the magnitude of A_2 agrees very well with Ref. 16. The resulting band structure of KCl is plotted in Fig. 14. We have indicated the extent of the convergence for the 9th and 10th bands at a few places in BZ

along Σ and Δ. The valence bands are consistent with the results of calculations using the APW method.[10] Our results for the conduction bands are similar to that obtained by the OPW method,[9] except that the energies have less dispersion as a function of wavevector. Figures 15 and 16 give the $\varepsilon_2(\omega)$ with constant matrix elements and with matrix elements computed from the pseudowavefunctions respectively. The scale factor used to reduce the main peak for the calculated ε_2 in Fig. 16 to the experimental value is 0.38. This was done to facilitate the comparison between theory and experiment. The decreasing of the scale factors from NaCl to KCl is consistent with the extent of the complication in the exciton structure; we shall discuss this point in Sec. IV. Because of the scale factor and the fact that the $\varepsilon_2(\omega)$ with matrix elements is only plotted up to 13 eV, the overall sum rule is not obeyed.

The prominent structure in the $\varepsilon_2(\omega)$ are listed in Table III. The exciton at the fundamental edge has been studied extensively.[2,3] The peak is at 7.5 eV (300°K), and the fundamental gap is placed at 8.69 eV. Our calculated $\varepsilon_2(\omega)$ starts at 8.67 eV with an M_o type singularity. For the experimental curve, the next structure is at 9.4 eV and is temperature dependent;[2,3] there is no corresponding peak in the spectrum of NaCl. It must, therefore, obviously be associated with the difference of the K^+ ion and the Na^+ ion as we mentioned in Sec. III A. We believe that the main difference is that the energies of the d-like conduction bands are lower with respect to the first conduction band in KCl than in NaCl. This structure is identified as an exciton associated with transitions at the X point, i.e. the X_3 exciton. Our calculation of $\varepsilon_2(\omega)$ does not include exciton effects

and therefore does not include this peak; however, the results of the band structure calculation supports the above identification. The conduction band at X_3 is the lowest energy band above the edge at Γ_1 (Fig. 14). The optical transition, $X_5' \rightarrow X_3$, is at an energy of 9.83 eV with cp symmetry M_0; it is followed by the $\Delta_5 \rightarrow \Delta_2'$ transition of M_1 type singularity at energy 10.1 eV. The binding energy of the X_3 exciton is of the order of 0.5 eV. The $L_3 \rightarrow L_2'$ transition is at 10.22 eV with an M_1 cp. There is no other cp along [111] direction as in the case of MgO[12] and NaCl for $4 \rightarrow 5$ transitions. The corresponding $X - \Delta - \Sigma$ peak in the other two crystals, MgO and NaCl, appears also in the present case. These transitions are $X_5' \rightarrow X_1$, $\Delta_5 \rightarrow \Delta_1$ and $\Sigma_4 \rightarrow \Sigma_1$ at energies 10.3 eV, 10.34 eV and 11.05 eV with M_0, M_1 and M_2 singularities. However, one cannot simply conclude that the peak at 10.35 eV in the calculated $\varepsilon_2(\omega)$ comes from the $X - \Delta - \Sigma$ transitions which are mainly $p \rightarrow s$ transitions, because forbidden transitions from $\Sigma_4 \rightarrow \Sigma_3$ occur at energy of 11.02 eV with cp symmetry M_2. We conclude, therefore, that the transitions $X_5' \rightarrow X_3$, $\Delta_5 \rightarrow \Delta_2'$ and $\Sigma_4 \rightarrow \Sigma_3$ together form another $X - \Delta - \Sigma$ structure which is composed mainly of $p \rightarrow d$ transitions contributing to the background of the 10.35 eV peak. If we project out the oscillator strengths of the $p \rightarrow d$ transitions and properly attribute them to the exciton structure at 9.4 eV, the strength of the calculated $\varepsilon_2(\omega)$ in the energy range between 10 eV and 11 eV would be decreased, and the agreement between theory and experiment would be better.

The next structure in the experimental spectrum is the hump at energies between 11.05 eV and 11.3 eV. The calculated $\varepsilon_2(\omega)$ shows the

hump beginning at 11.18 eV and ending at 11.45 eV. the cp's contributing in this region come mainly from $\Gamma_{15} \rightarrow \Gamma_{25}'$ and $\Gamma_{15} \rightarrow \Gamma_{12}$ with M_0 type singularities for both transitions. The $\Gamma_{15} \rightarrow \Gamma_{25}'$ transition from 4th to 6th bands has no cp, because the interband energies at the neighboring points in k-space show a maximum at Γ when one approaches Γ along Δ and Σ and a minimum when one approaches Γ along Λ.

The main peak in the calculated spectrum is at 11.75 eV which is 0.75 eV lower in energy when compared with the 12.5 eV peak in the experimental curve. This kind of discrepancy between theory and experiment happens in NaCl also; we expect this discrepancy is caused for the same reason as given for NaCl in Sec. II. Most of the contribution to this peak is from $3 \rightarrow 7$ and $4 \rightarrow 7$ transitions inside the BZ near Σ. The higher energy cp's are listed in Table III up to 13 eV only.

IV. Comparison of NaCl and KCl

The band structures for the two crystals show many common characteristics. For example, the two valence bands are almost identical; there is less dispersion in the energy with respect to wavevector as compared to many other crystals, e.g., III - V, II - VI compounds.[12,15] The exciton at the band edge of the two crystals is similar;[2,3] the binding energy is of the order of 1 eV.

However, the measured and calculated spectra also show distinct differences. The sharp peak at 9.4 eV in KCl, which is temperature dependent,[2,3] does not have a counterpart in NaCl. We have discussed its origin in Sec. III. It is this extra exciton peak which causes the overall scale factor of $\varepsilon_2(\omega)$ in KCl to be 36% lower than in NaCl. As we have mentioned in Sec. III, this exciton structure is associated

with the lowering of the X_3 state in KCl. This lowering effect does not, in fact, involve the X_3 state only. All the d-like conduction bands will have lower energy with respect to the s-like conduction band when compared with the results of NaCl. So the major difference of the two band structures is exhibited in the relative energies of the conduction bands with s and d characteristics. Two places in the BZ at which this effect is most prominent are at Γ and X. In KCl, the lowering of the Γ_{25}' and Γ_{12} bands with respect to the Γ_1 band are 1.33 eV and 1.62 eV respectively. Moreover, the X_3 band is even lower than the X_1 band (by 0.47 eV) and is the second lowest conduction band. However, the X_3 band in NaCl is nearly degenerate with the X_1 band and is higher than the L_2' band. As a result of this lowering of the d-like conduction bands in KCl, the symmetries of the cp's at Λ (4 → 5) and Γ (4 → 6) are changed. Along Λ, the upper Λ_1 (6th band near Γ_{25}') state is brought down along with the Γ_{25}' state. The two Λ_1 bands repel each other so that the 5th band is pushed down slightly and the associated M_1 cp is moved over to the edge of the BZ. The complication of the cp for 4 → 6 transition at Γ is affected by the lowering of the 6th band along Δ and Σ.

We have extracted the Cl^- potential from the calculations for NaCl and KCl and we have scaled the one obtained from NaCl to the lattice constant of KCl. The results are given in Fig. 17.

In summary we see that the local pseudopotential Hamiltonian gives a good band structure for NaCl as is demonstrated by the fact that the $\varepsilon_2(\omega)$ and the conduction band density states calculated from the band structure agree quite well with the uv optical data[2,3] and the soft

x-ray photoabsorption measurements.[11] The results on KCl should be considered as preliminary because the form of the nonlocal pseudopotential causes a problem of convergence for the eigenvalues at higher energies. Nevertheless, we can still deduce at least important features: a. The calculation shows that one needs to put a nonlocal pseudopotential term for the d-like states which do not have strong core cancellation but are important for the electronic properties in the insulator as well as in the metal.[16] b. It gives an indication of how high energy exciton structure affects the optical properties of alkali-halides.

ACKNOWLEDGMENTS

We would like to thank Professor W. C. Walker and Dr. D. M. Roessler for sending us their data prior to publication. We wish to thank Professor L. M. Falicov for his help with the $\ell = 2$ nonlocal pseudopotential and Professor J. C. Phillips for helpful discussions. One of us, C. Y. F., would like to thank Miss Y. Tung and Mr. J. Walter for checking the computer program and for many helpful discussions.

This work was done under the auspices of the United States Atomic Energy Commission.

REFERENCES

1. R. Hilsch and R. W. Pohl, Z. Physik, 59, 812 (1930); E. G. Schneider and H. M. O'Bryan, Phys. Rev. 51, 293 (1937); J. E. Eby, K. J. Teegarden and D. B. Dutton, ibid., 116, 1099 (1959); K. J. Teegarden and G. Baldini, ibid., 155, 896 (1967); F. Fisher and R. Hilsch, Nachtr. Akad. Wiss. Goettingen, II, Math. Physik. Kl. 8, 241 (1959); F. Fisher, Z. Physik, 160 194 (1960).
2. P. L. Hartman, J. R. Nelson and J. G. Seigfried, Phys. Rev. 105 123 (1967); J. W. Taylor and P. L. Hartman, ibid., 113, 1421 (1959); H. R. Phillipp and H. Ehrenreich, ibid., 131, 2016 (1963); T. Tomiki, J. Phys. Soc. Japan 22, 463 (1967); G. Baldini and B. Basacchi, Phys. Rev. 166, 863 (1968).
3. D. M. Roessler and W. C. Walker, Phys. Rev. 166, 599 (1968).
4. W. Shockley, Phys. Rev. 50, 754 (1936).
5. S. R. Tibbs, Trans. Faraday Soc. 35, 1471 (1939).
6. R. C. Casella, Phys. Rev. 104, 1260 (1956).
7. C. Y. Fong and M. L. Cohen, Phys. Rev. Letts. 20, 22 (1968).
8. L. P. Howland, Phys. Rev. 109, 1927 (1958).
9. S. Oyama and T. Miyakawa, J. Phys. Soc. Japan 21, 865 (1966).
10. P. D. Decicco, Phys. Rev. 153, 931 (1967).
11. R. Haensel, C. Kunz, T. Sasaki and B. Sonntag, Phys. Rev. Letts. 20, 1436 (1968).
12. C. Y. Fong, W. Saslow and M. L. Cohen, Phys. Rev. 168, 992 (1968).
13. T. K. Bergstresser, W. Saslow, C. Y. Fong, M. L. Cohen and D. Brust, Solid State Comm. 5, 667 (1967).
14. J. P. Walter and M. L. Cohen, (to be published).

15. M. L. Cohen and T. K. Bergstresser, Phys. Rev. 141, 789 (1966).

16. M. J. G. Lee and L. M. Falicov, Proc. Roy. Soc. A 304, 319 (1968).

17. C. Kittel, Introduction to Solid State Physics, 3rd edition, p. 105, John Wiley and Sons, Inc. New York (1966).

TABLE CAPTIONS

Table I. Interband critical points for NaCl with energy from 8 to 18 eV.

Table II. Form factors of KCl (in Ry.).

Table III. Prominent interband transitions for KCl.

FIGURE CAPTIONS

Fig. 1. Band structure of NaCl.

Fig. 2. Theoretical $\varepsilon_2(\omega)$ of NaCl with matrix elements computed from pseudowavefunctions.

Fig. 3. Theoretical $\varepsilon_2(\omega)$ of NaCl with constant matrix elements.

Fig. 4. Energy contours of NaCl for 4 → 5 transitions in the ΓKL and ΓKWX planes

Fig. 5. Energy contours of NaCl for 4 → 6 transitions in the ΓKL and ΓKWX planes.

Fig. 6. Energy contours of NaCl for 4 → 7 transitions in the ΓKL and ΓKWX planes.

Fig. 7. Energy contours of NaCl for 3 → 5 transitions in the ΓKL and ΓKWX planes.

Fig. 8. Energy contours of NaCl for 3 → 6 transitions in the ΓKL and ΓKWX planes.

Fig. 9. Energy contours of NaCl for 3 → 7 transitions in the ΓKL and ΓKWX planes.

Fig. 10. Energy contours of NaCl for 2 → 5 transitions in the ΓKL and ΓKWX planes.

Fig. 11. Energy contours of NaCl for 2 → 6 transitions in the ΓKL and ΓKWX planes.

Fig. 12. Energy contours of NaCl for 2 → 7 transitions in the ΓKL and ΓKWX planes.

Fig. 13. Conduction band density of states for NaCl.

Fig. 14. Band structure of KCl.

Fig. 15. Theoretical $\varepsilon_2(\omega)$ of KCl with constant matrix elements.

Fig. 16. Theoretical $\varepsilon_2(\omega)$ of KCl with matrix elements computed from pseudowavefunctions. (The overall scale factor is 0.38.)

FIGURE CAPTIONS, cont.

17. Comparison of Cl^- potentials extracted from NaCl and KCl.

TABLE I

Calculated Critical Point Energy (eV)	Band Transitions	Symmetry
8.97	$\Gamma_{15} \rightarrow \Gamma_1$	M_0
9.86	$L_3 \rightarrow L_2'$	M_0
10.29	$\Lambda_3 \rightarrow \Lambda_1$	M_2 (4→5)
10.35	$X_5' \rightarrow X_3$	M_0
10.43	$X_5' \rightarrow X_1$	M_0
11.07	$\Delta_5 \rightarrow \Delta_1$	M_1 (4→5),(3→5)
11.25	$L_1 \rightarrow L_2'$	M_1
11.32	$\Sigma_4 \rightarrow \Sigma_1$	M_2 (4→5)
11.33	$X_4' \rightarrow X_3$	M_0
11.41	$X_4' \rightarrow X_1$	M_0
11.64	$\Delta_1 \rightarrow \Delta_1$	M_1 (2→5)
	$\Delta_1 \rightarrow \Delta_2'$	M_0 (2→6) (forbidden)
11.74	$\Delta_1 \rightarrow \Delta_1$	M_1 (2→6)
11.74	$\Sigma_4 \rightarrow \Sigma_3$	M_1 (forbidden)
11.82	$\Sigma_3 \rightarrow \Sigma_1$	M_2 (3→5)
12.04	$\Sigma_3 \rightarrow \Sigma_3$	M_1
12.1	W	M_3 (4→5)
12.24	$\Sigma_1 \rightarrow \Sigma_1$	M_2 (2→5)
12.26	$L_3 \rightarrow L_3'$	M_1 (4→6)
		M_0 (4→7), (3→6), (3→7)
12.4	$\Sigma_1 \rightarrow \Sigma_3$	M_1
12.6	W	M_3 (3→5), (2→5)
12.61	$\Lambda_1 \rightarrow \Lambda_1$	M_2 (2→6)
12.64	$\Delta_5 \rightarrow \Delta_1$	M_2 (4→7)

TABLE I (cont.)

Calculated Critical Point Energy (eV)	Band Transitions	Symmetry
12.66	$\Lambda_3 \rightarrow \Lambda_3$	M_3 (4→6)
12.67	$\Gamma_{15} \rightarrow \Gamma_{25}'$	M_0
12.7	$\Sigma_4 \rightarrow \Sigma_1$	M_1 (4→7)
12.71	$\Lambda_3 \rightarrow \Lambda_1$	M_3 (4→6), (3→6)
12.77	$\Delta_5 \rightarrow \Delta_2'$	M_1
12.79	$\Sigma_4 \rightarrow \Sigma_3$	M_3 (forbidden)
12.8	$\Delta_5 \rightarrow \Delta_2'$	M_1
12.82	$\Sigma_3 \rightarrow \Sigma_3$	M_3
12.83	$\Lambda_1 \rightarrow \Lambda_1$	M_2 (2→6)
12.86	$\Sigma_1 \rightarrow \Sigma_3$	M_3
12.89	$\Sigma_4 \rightarrow \Sigma_1$	M_1 (4→7)
12.95	$\Lambda_3 \rightarrow \Lambda_3$	M_3 (4→7) M_2 (3→7)
12.99	$\Sigma_4 \rightarrow \Sigma_1$	M_3 (4→6)
13.	$\Sigma_3 \rightarrow \Sigma_1$	M_1 (3→7)
13.13	$\Delta_5 \rightarrow \Delta_1$	M_3 (4→7)
13.02	$\Sigma_3 \rightarrow \Sigma_1$	M_3 (3→7)
13.05	$\Delta_1 \rightarrow \Delta_1$	M_0 (2→7)
13.13	$\Delta_5 \rightarrow \Delta_1$	M_3
13.24	$\Delta_1 \rightarrow \Delta_1$	M_3 (2→7)
13.64	$L_1 \rightarrow L_3$	M_3 (2→6) M_1 (2→7) (forbidden)
13.64	$\Sigma_3 \rightarrow \Sigma_1$	M_3 (3→6)

TABLE I (cont.)

Calculated Critical Point Energy (eV)	Band Transitions	Symmetry
13.64	W	M_3
13.77	$\Sigma_1 \rightarrow \Sigma_1$	M_3

TABLE II

Form Factors	Numerical Values
$V^S(200)$	- .1012 R_y
$V^S(220)$	- .0321
$V^S(222)$	.0073
$V^A(111)$	.1243
$V^A(311)$	- .0322
V^d	-2.5958

TABLE III

Calculated Important Critical Point Energy (eV)	Band Transitions	Symmetry
8.67	$\Gamma_{15} \rightarrow \Gamma_1$	M_0
9.83	$X_5' \rightarrow X_3$	M_0
10.1	$\Delta_5 \rightarrow \Delta_2'$	M_1
10.22	$L_3 \rightarrow L_2'$	M_1
10.3	$X_5' \rightarrow X_1$	M_0
10.34	$\Delta_5 \rightarrow \Delta_1$	M_1
11.02	$\Sigma_4 \rightarrow \Sigma_3$	M_2 (forbidden)
11.05	$\Sigma_4 \rightarrow \Sigma_1$	M_2 $(4 \rightarrow 5)$
11.05	$\Gamma_{15} \rightarrow \Gamma_{25}'$	M_0 $(2 \rightarrow 6)$, $(2 \rightarrow 7)$, $(2 \rightarrow 8)$; $(3 \rightarrow 7)$, $(3 \rightarrow 8)$; $(4 \rightarrow 7)$, $(4 \rightarrow 8)$.
11.26	$\Gamma_{15} \rightarrow \Gamma_{12}$	M_0 $(2 \rightarrow 8)$, $(2 \rightarrow 9)$; $(3 \rightarrow 8)$, $(3 \rightarrow 9)$; $(4 \rightarrow 8)$, $(4 \rightarrow 9)$.
11.56	$\Sigma_4 \rightarrow \Sigma_2$	M_1
12.19	$L_3 \rightarrow L_3'$	M_3 $(4 \rightarrow 6)$; M_2 $(3 \rightarrow 6)$; M_1 $(4 \rightarrow 7)$, $(3 \rightarrow 7)$.

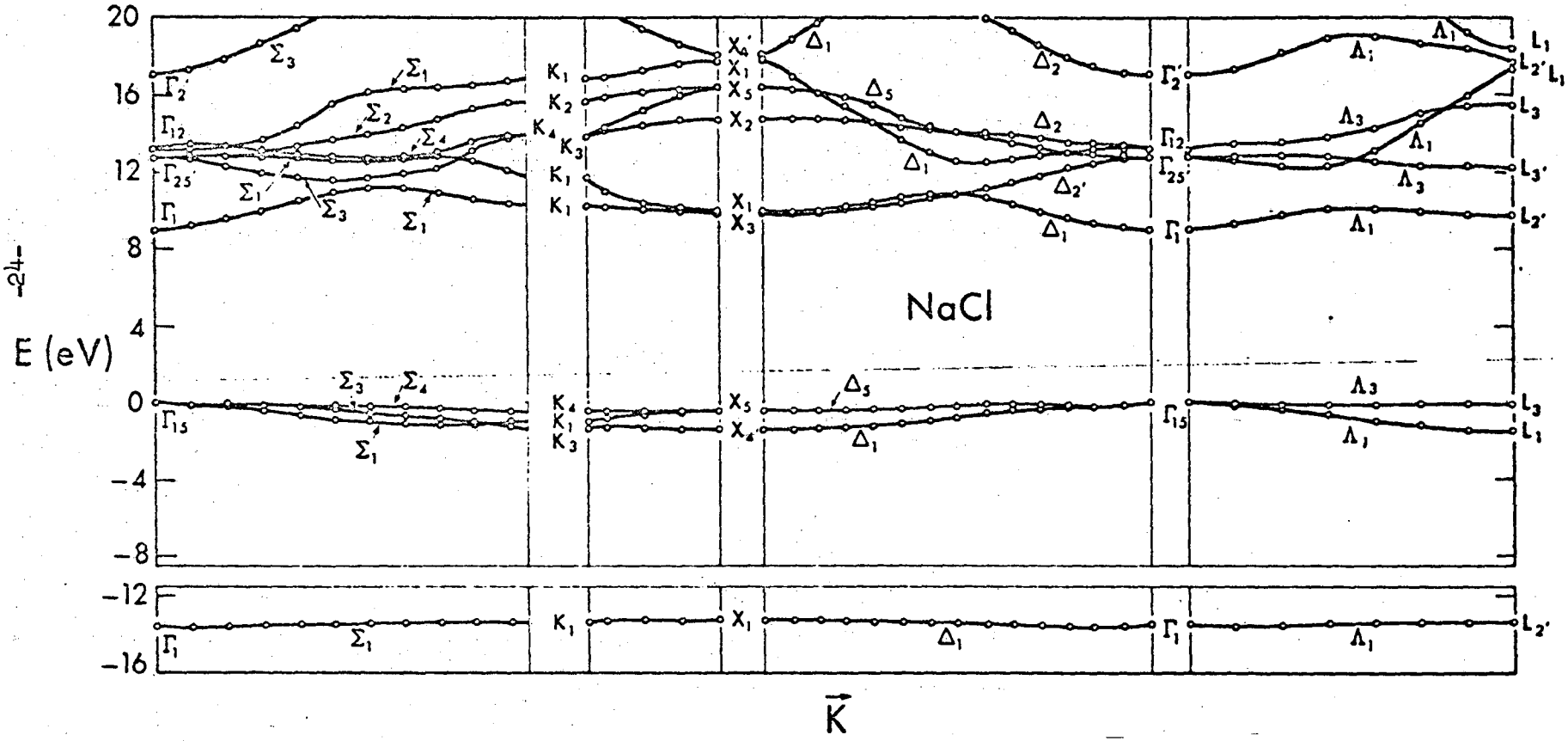
NaCl
E (eV)
20
16
12
8
4
0
−4
−8
−12
−16
$\vec{K}$
Γ_2'
Γ_{12}
Γ_{25}'
Γ_1
Γ_{15}
Σ_1
Σ_2
Σ_3
Σ_4
K_1
K_2
K_3
K_4
X_4'
X_1
X_5
X_2
X_3
X_4
Δ_1
Δ_2
Δ_5
Δ_2'
Λ_1
Λ_3
L_1
L_2'
L_3
L_3'

Fig. 1

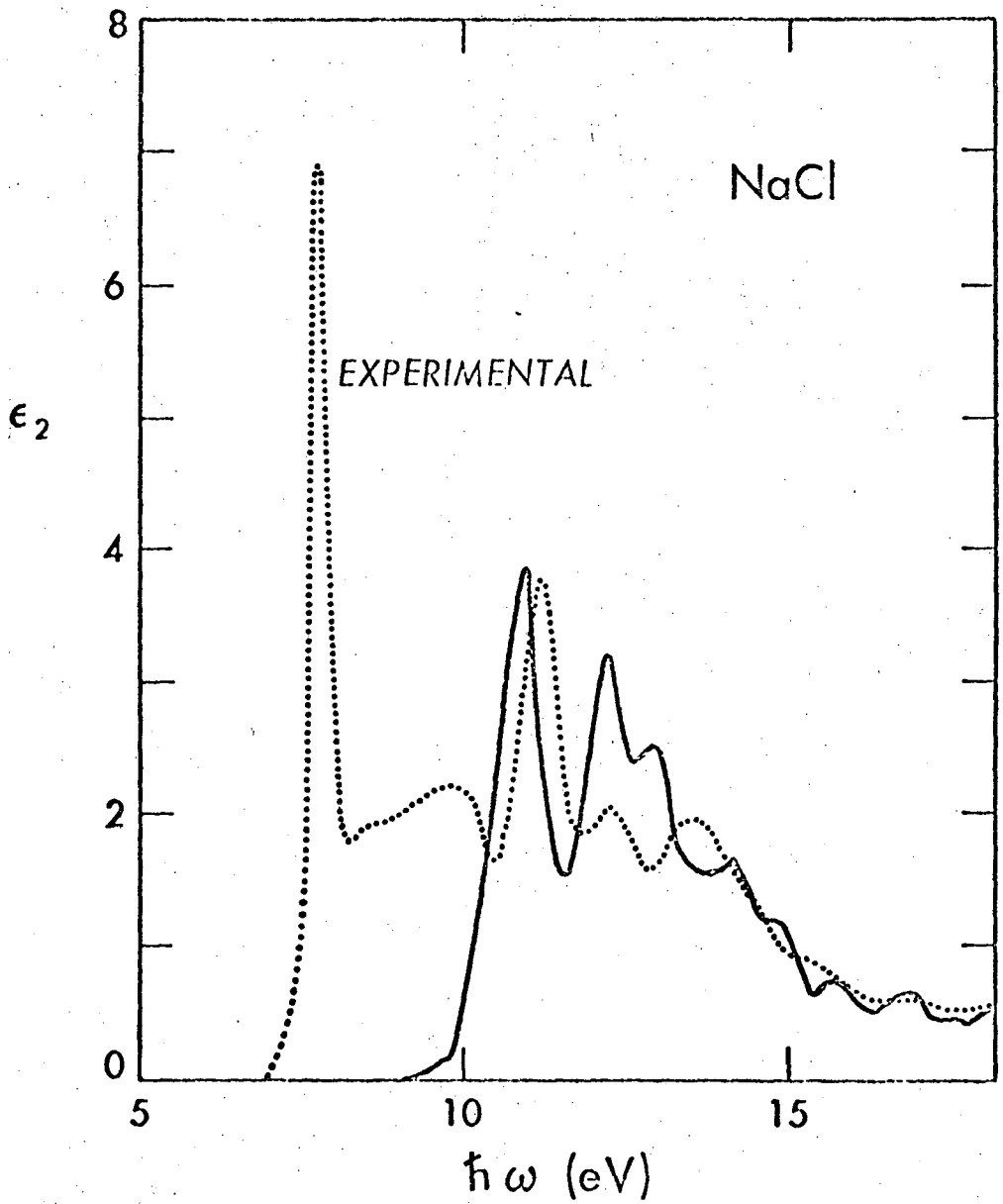

Fig. 2.

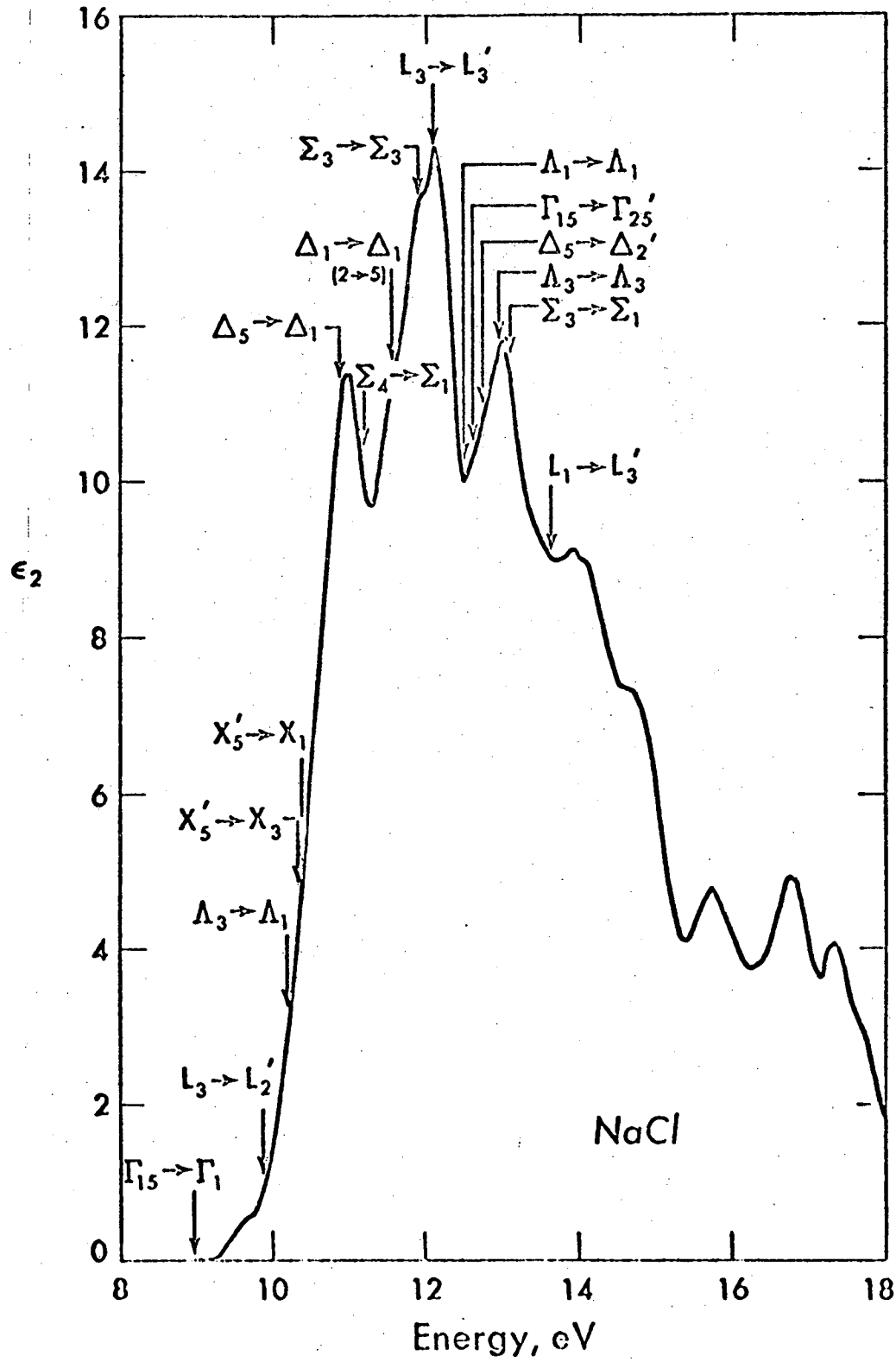
16
14
12
10
8
6
4
2
0
ϵ_2
8
10
12
14
16
18
Energy, eV
$L_3 \rightarrow L_3'$
$\Sigma_3 \rightarrow \Sigma_3$
$\Lambda_1 \rightarrow \Lambda_1$
$\Gamma_{15} \rightarrow \Gamma_{25}'$
$\Delta_5 \rightarrow \Delta_2'$
$\Lambda_3 \rightarrow \Lambda_3$
$\Sigma_3 \rightarrow \Sigma_1$
$\Delta_1 \rightarrow \Delta_1$
(2→5)
$\Delta_5 \rightarrow \Delta_1$
$\Sigma_4 \rightarrow \Sigma_1$
$L_1 \rightarrow L_3'$
$X_5' \rightarrow X_1$
$X_5' \rightarrow X_3$
$\Lambda_3 \rightarrow \Lambda_1$
$L_3 \rightarrow L_2'$
$\Gamma_{15} \rightarrow \Gamma_1$
NaCl

Fig. 3

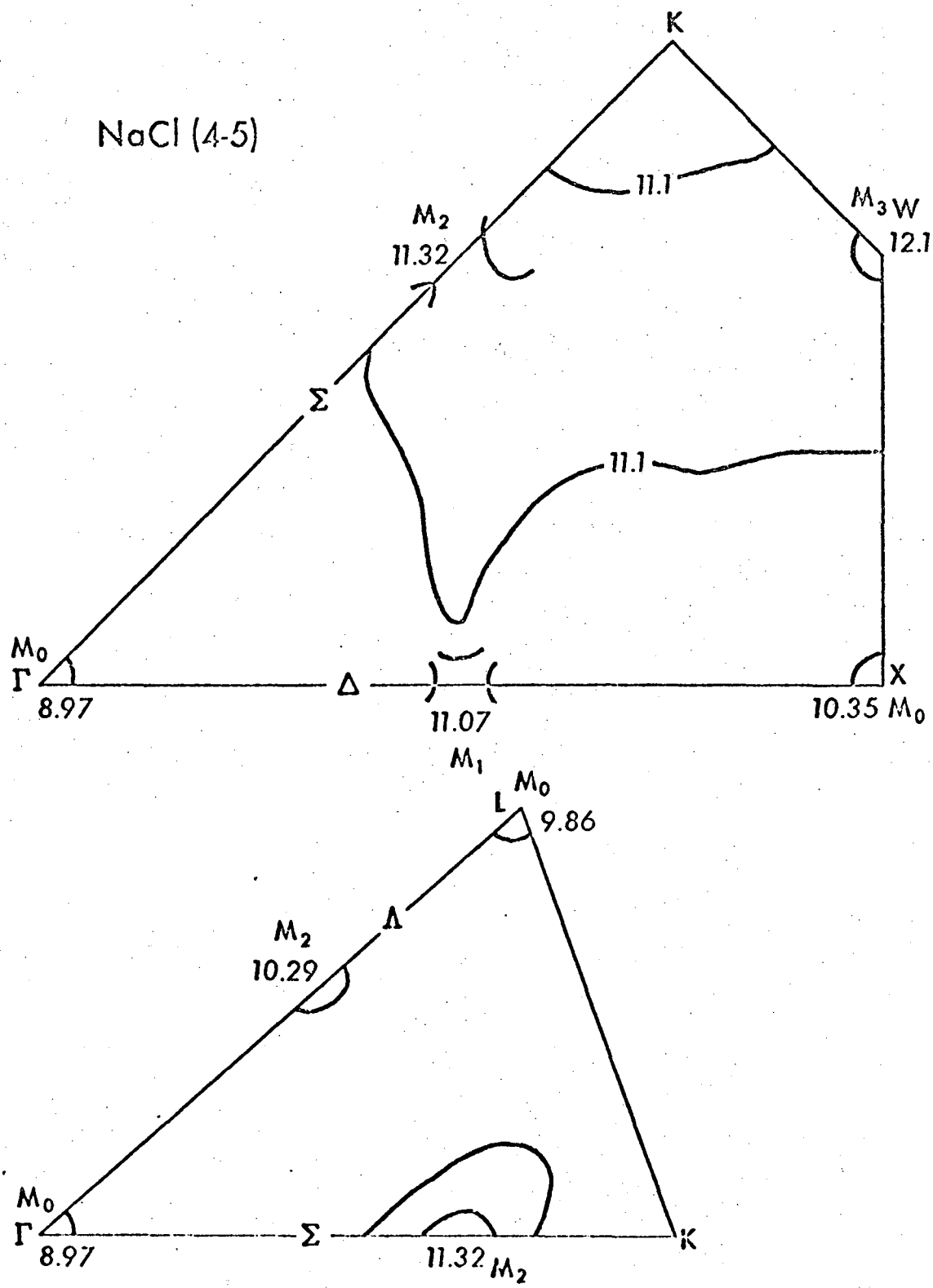
NaCl (4-5)
K
11.1
M2
11.32
M3 W
12.1
Σ
11.1
M0
Γ
8.97
Δ
11.07
X
10.35 M0
M1
M0
L
9.86
Λ
M2
10.29
M0
Γ
8.97
Σ
11.32 M2
K

Fig. 4

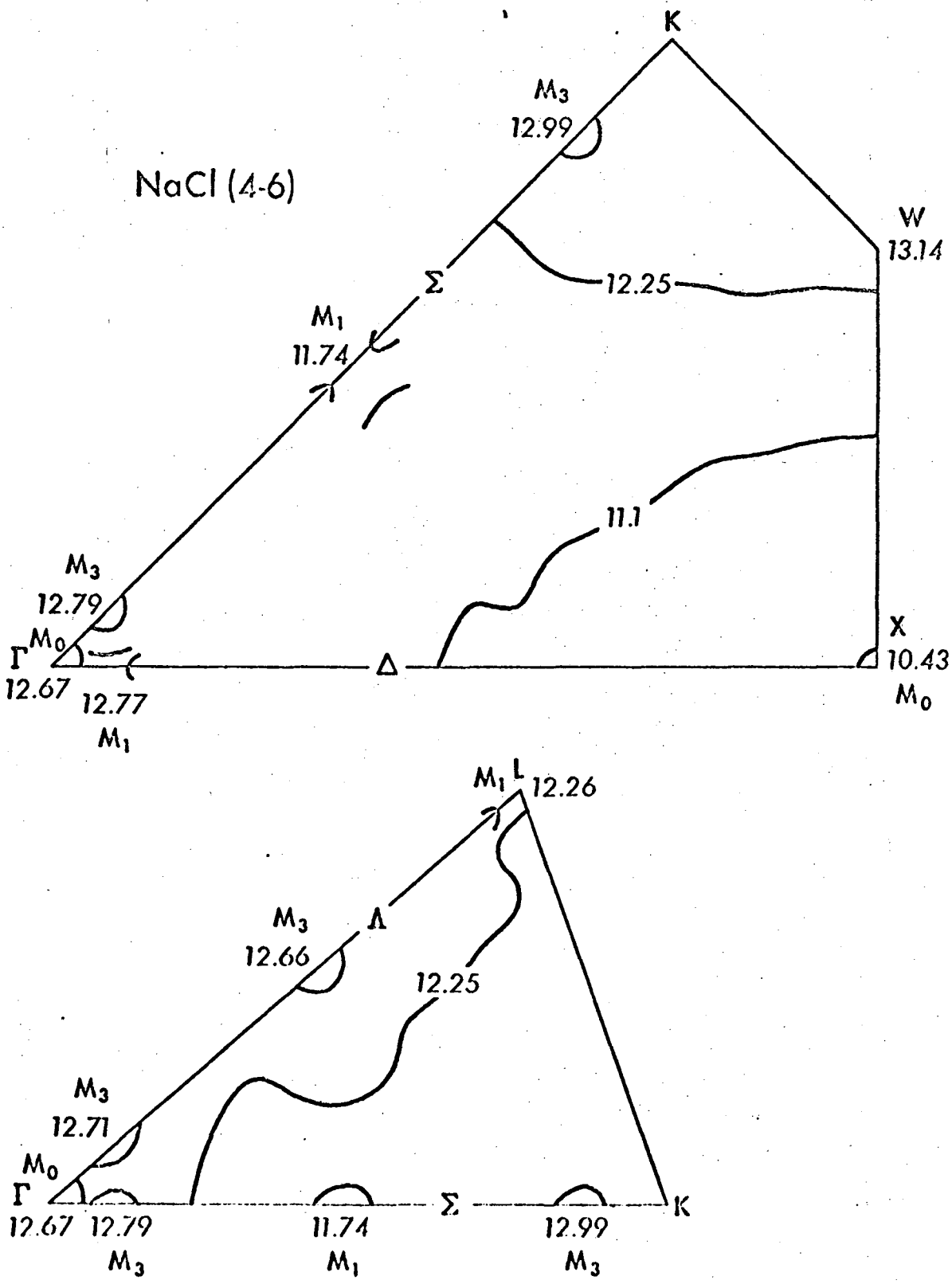
NaCl (4-6)
K
M3
12.99
W
13.14
Σ
12.25
M1
11.74
11.1
M3
12.79
M0
Γ
12.67
12.77
M1
Δ
X
10.43
M0
M1
L
12.26
M3
12.66
Λ
12.25
M3
12.71
M0
Γ
12.67
12.79
M3
Σ
11.74
M1
K
12.99
M3

Fig. 5

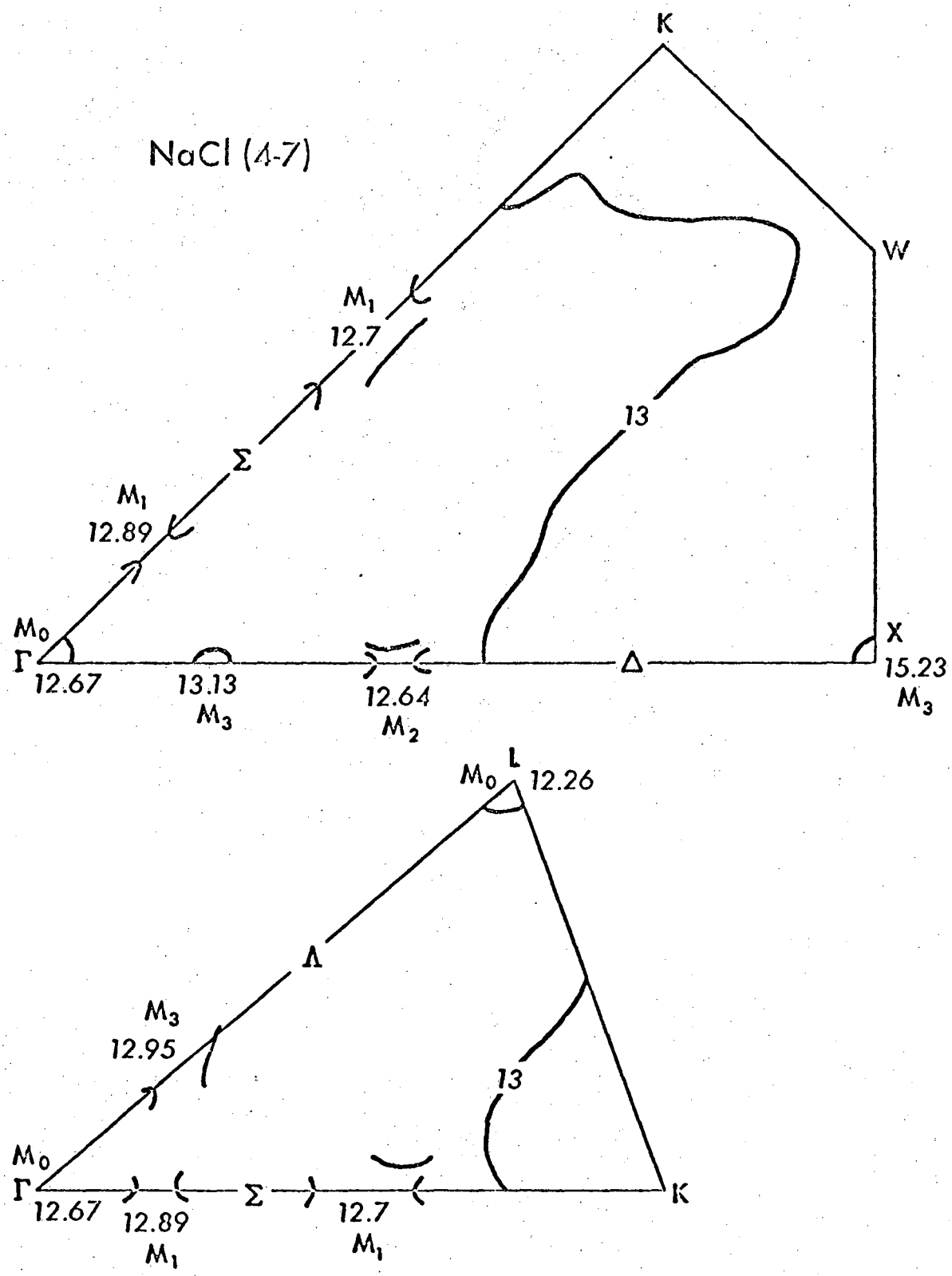
NaCl (4-7)
K
W
M_1
12.7
13
Σ
M_1
12.89
M_0
Γ
12.67
13.13
M_3
12.64
M_2
Δ
X
15.23
M_3
L
M_0
12.26
Λ
M_3
12.95
13
M_0
Γ
12.67
12.89
M_1
Σ
12.7
M_1
K

Fig. 6

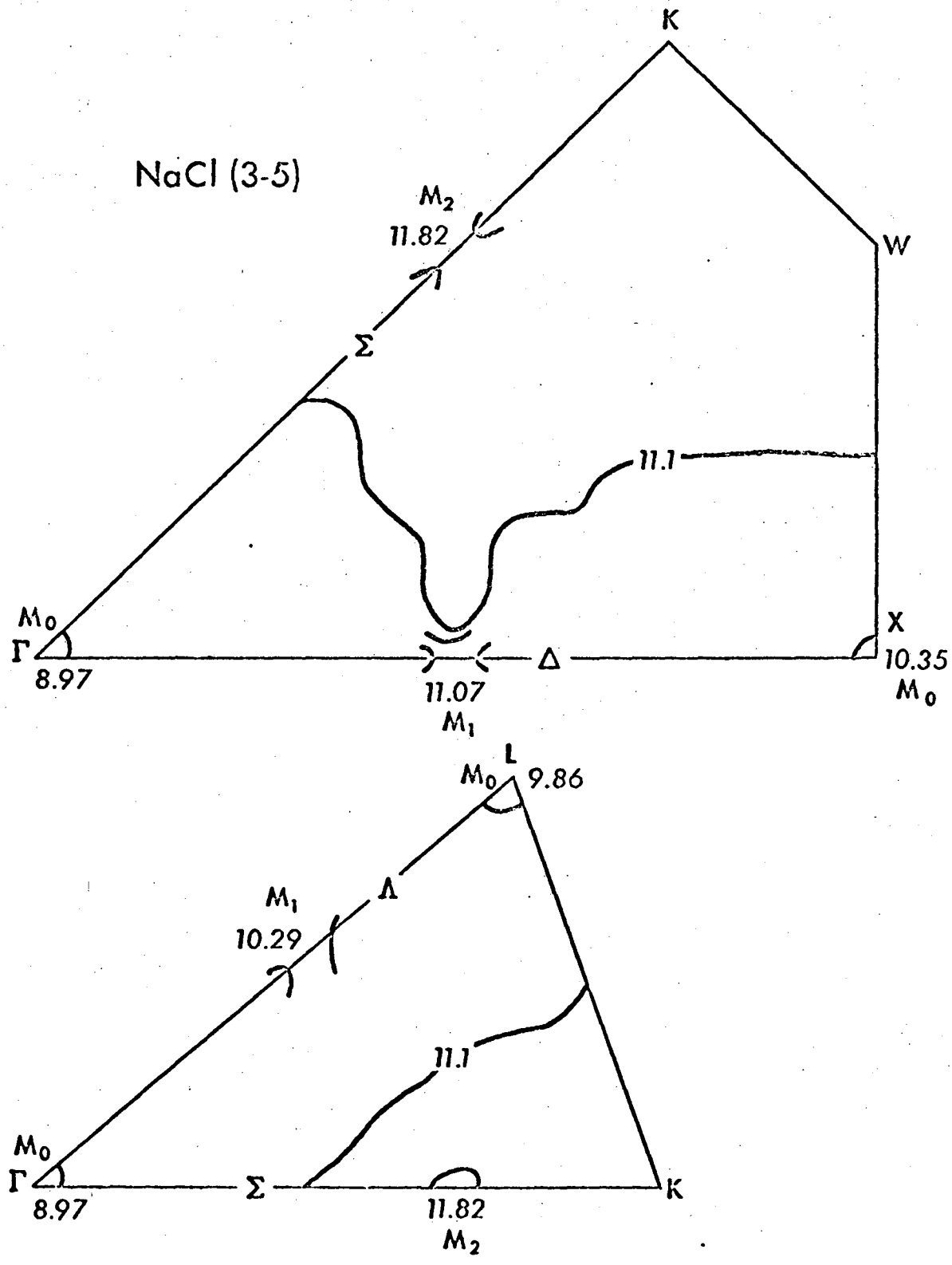
NaCl (3-5)
K
W
M_2
11.82
Σ
11.1
M_0
Γ
8.97
Δ
11.07
M_1
X
10.35
M_0
L
M_0
9.86
Λ
M_1
10.29
11.1
M_0
Γ
8.97
Σ
11.82
M_2
K

Fig. 7

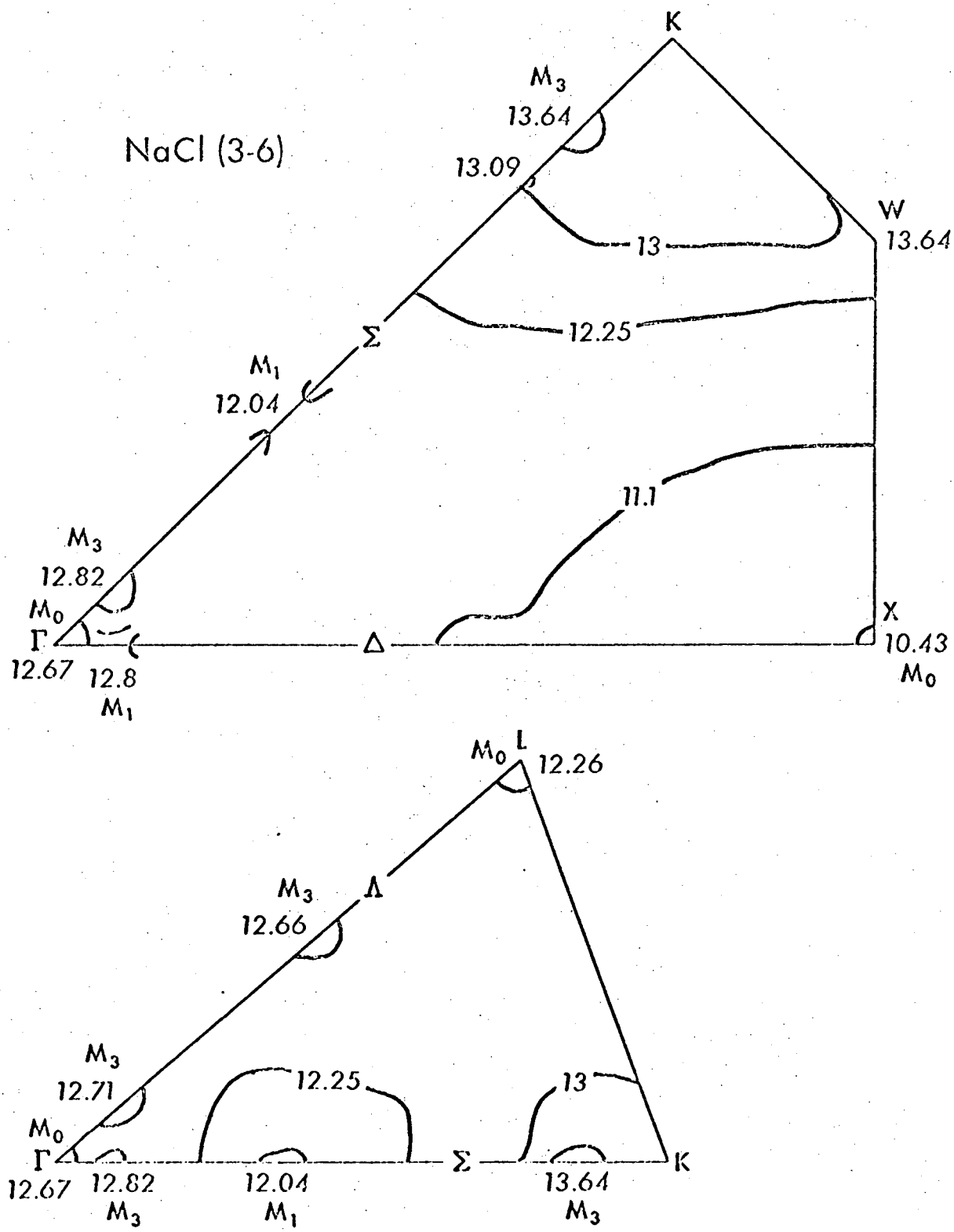
NaCl (3-6)
K
M3
13.64
13.09
W
13.64
13
12.25
Σ
M1
12.04
11.1
M3
12.82
M0
Γ
12.67
12.8
M1
Δ
X
10.43
M0
M0
L
12.26
M3
Λ
12.66
M3
12.71
M0
Γ
12.67
12.82
M3
12.25
12.04
M1
Σ
13
13.64
M3
K

Fig. 8

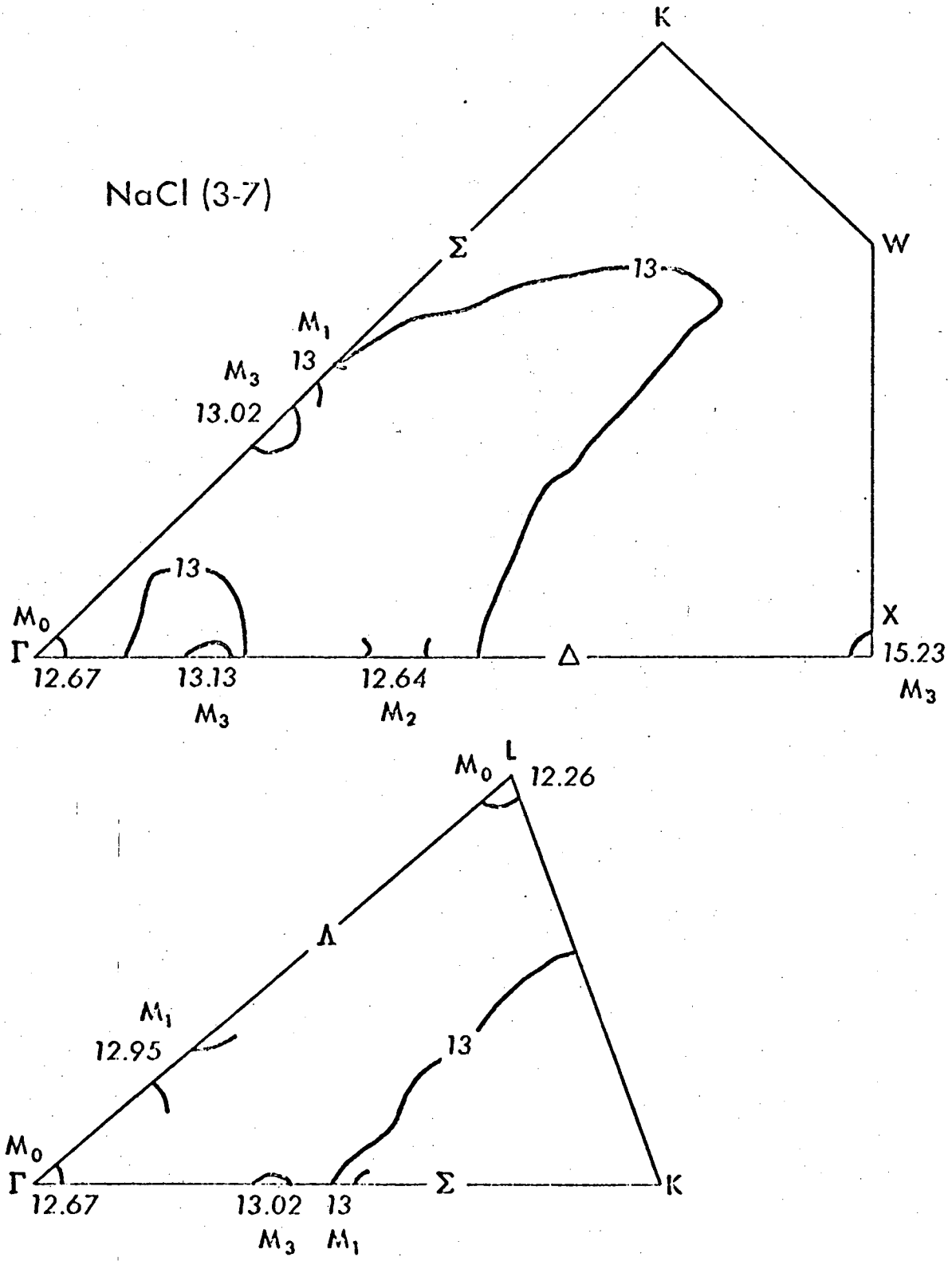
NaCl (3-7)
K
Σ
W
13
M1
13
M3
13.02
13
M0
Γ
12.67
13.13
M3
12.64
M2
Δ
X
15.23
M3
M0
L
12.26
Λ
M1
12.95
13
M0
Γ
12.67
13.02
M3
13
M1
Σ
K

Fig 9

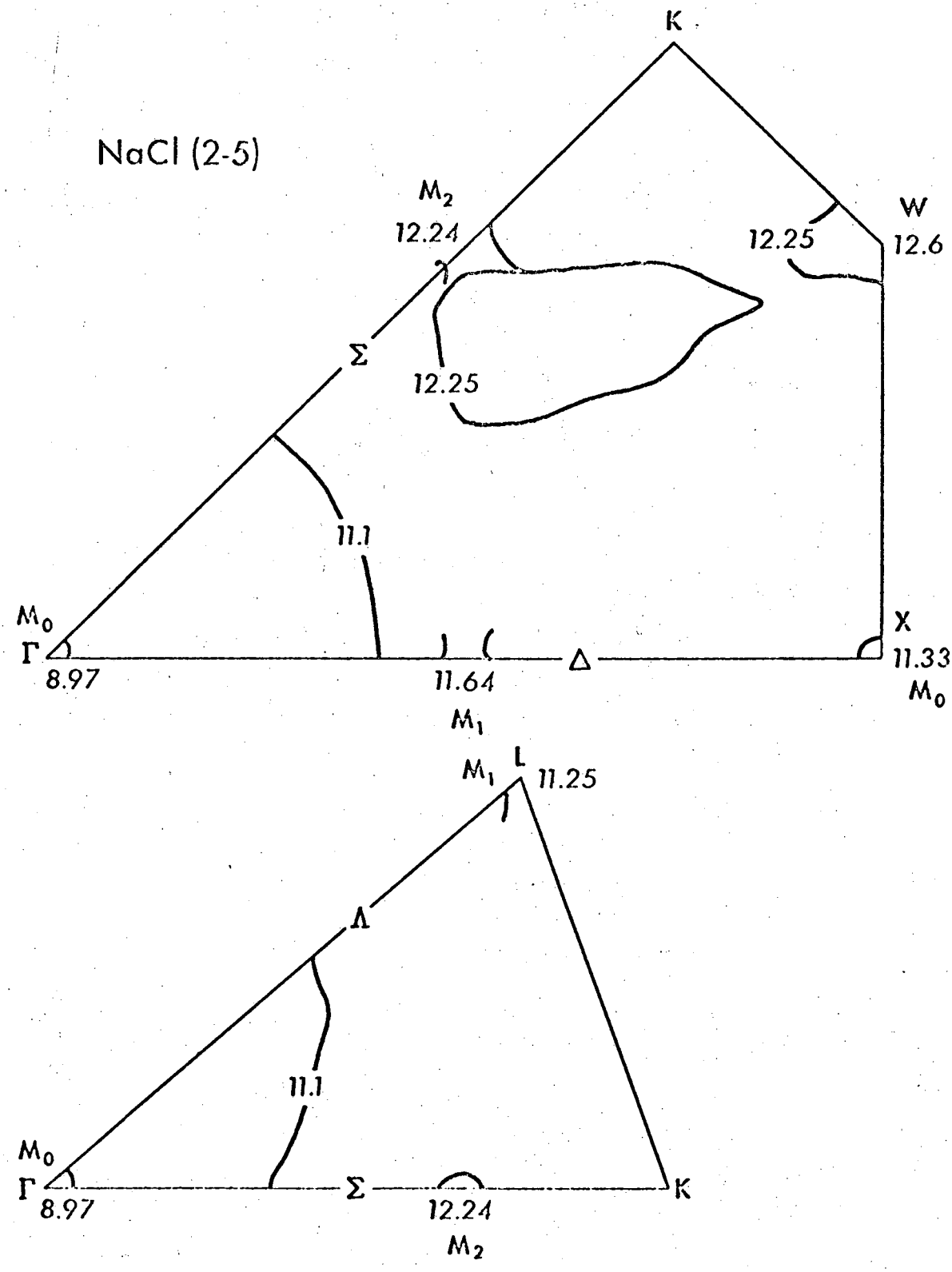
NaCl (2-5)
K
M_2
12.24
W
12.25
12.6
Σ
12.25
11.1
M_0
Γ
8.97
11.64
Δ
X
11.33
M_0
M_1
M_1
L
11.25
Λ
11.1
M_0
Γ
8.97
Σ
12.24
M_2
K

Fig. 10

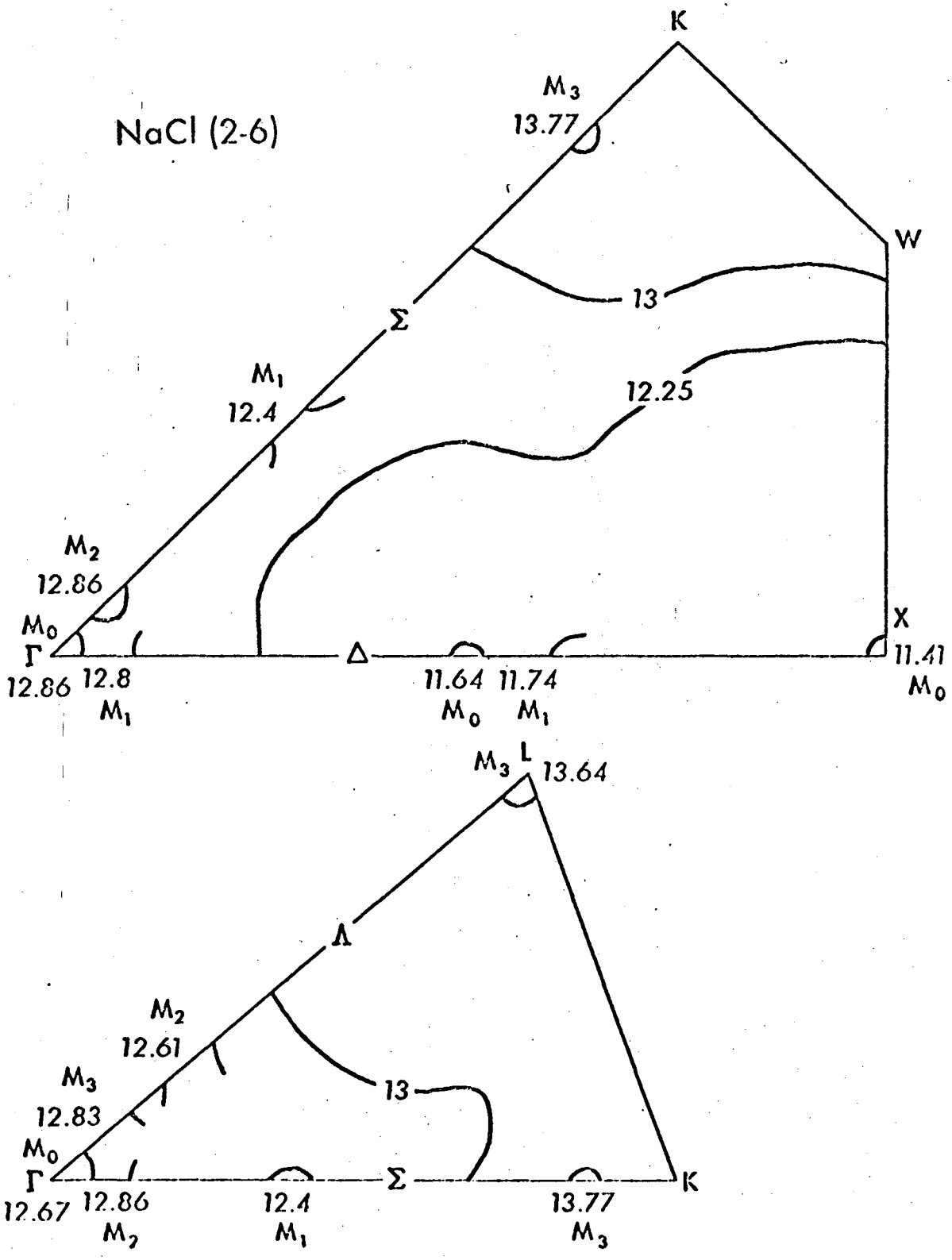
NaCl (2-6)
K
M3
13.77
W
13
Σ
M1
12.4
12.25
M2
12.86
M0
Γ
Δ
X
11.41
M0
12.86
12.8
M1
11.64
M0
11.74
M1
M3
L
13.64
Λ
M2
12.61
13
M3
12.83
M0
Γ
Σ
K
12.67
12.86
M2
12.4
M1
13.77
M3

Fig. 11

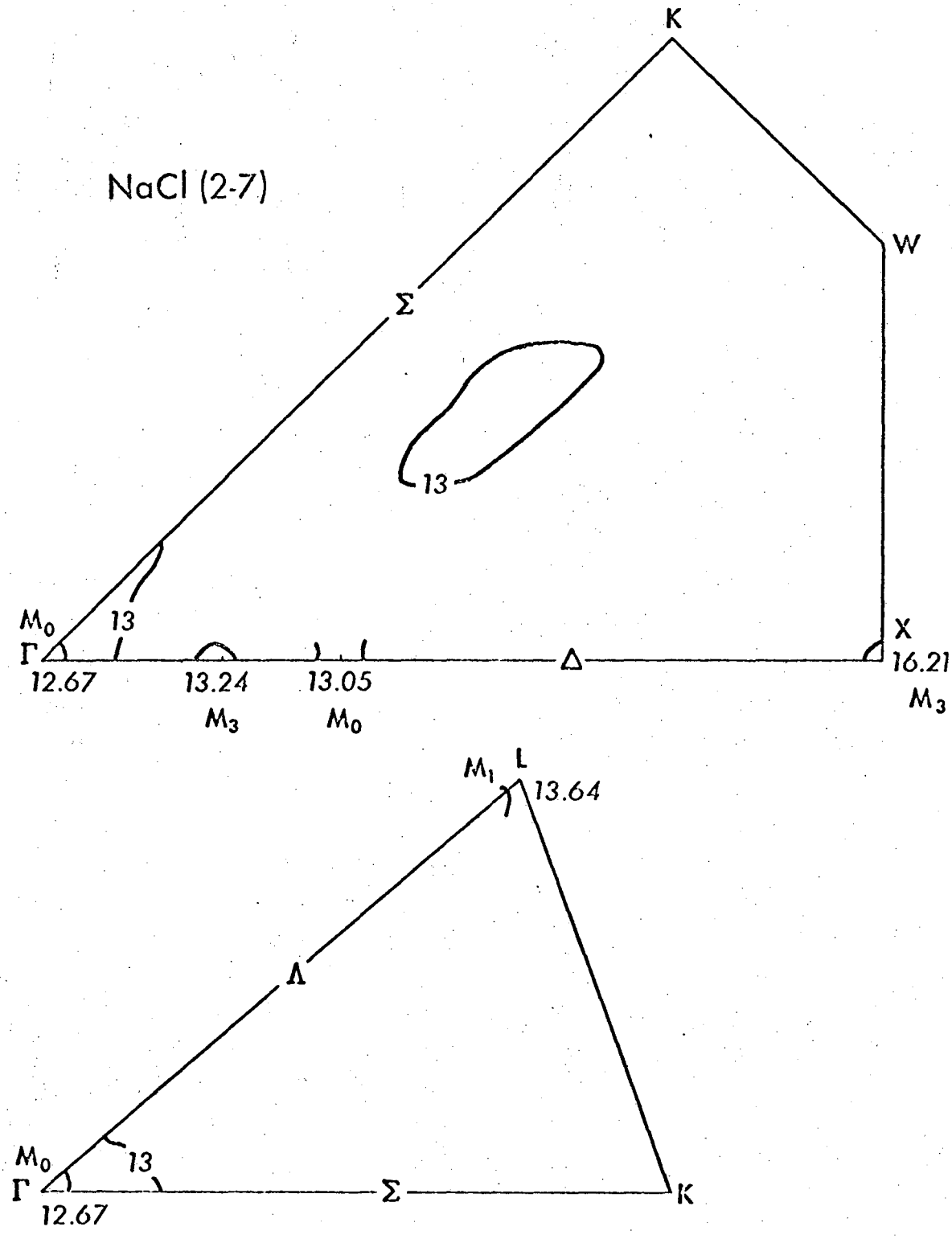
NaCl (2-7)
K
W
Σ
13
M0
Γ
13
12.67
13.24
M3
13.05
M0
Δ
X
16.21
M3
M1
L
13.64
Λ
M0
Γ
13
12.67
Σ
K

Fig. 12

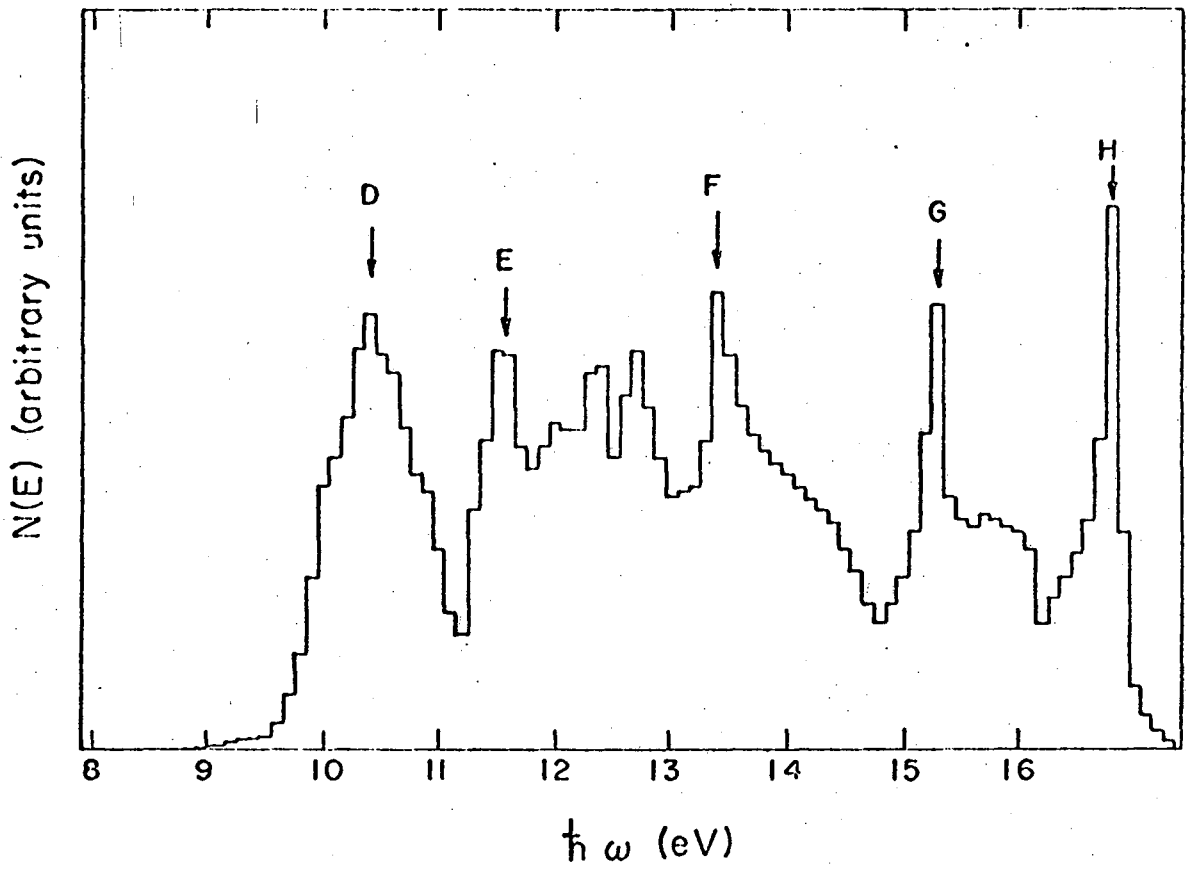

XBL6812-7328

Fig. 13

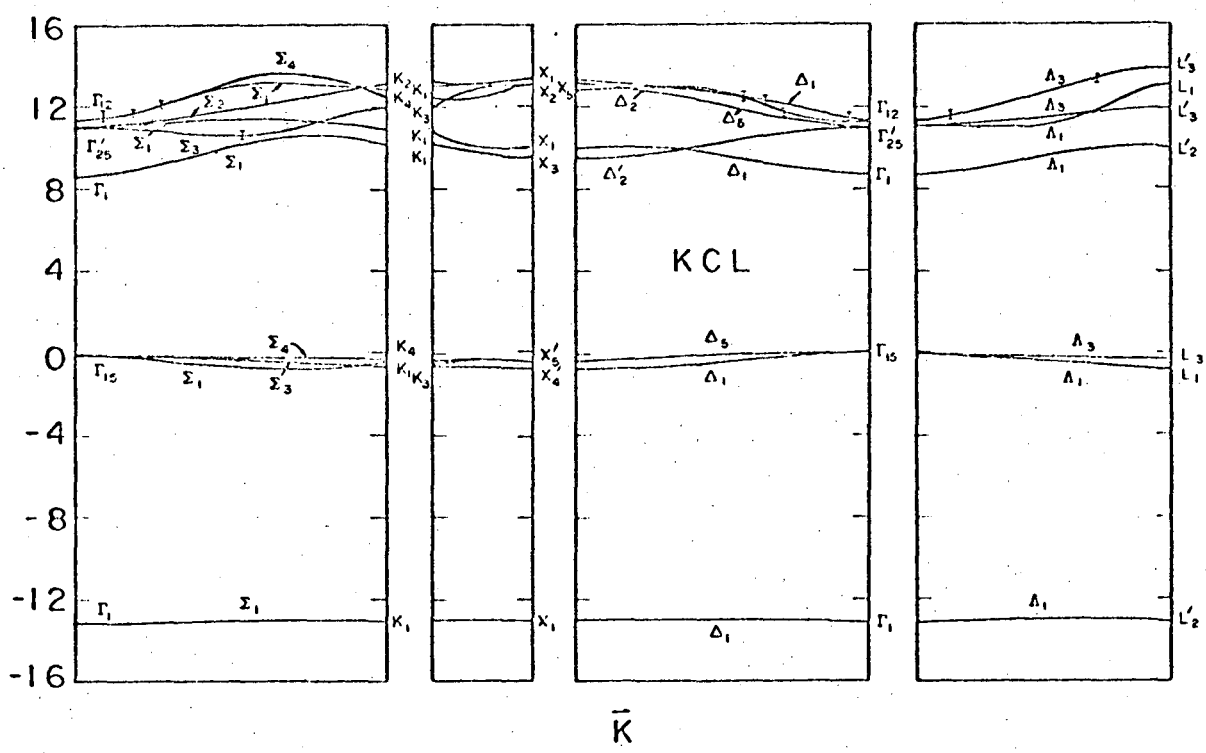

Fig 1-1

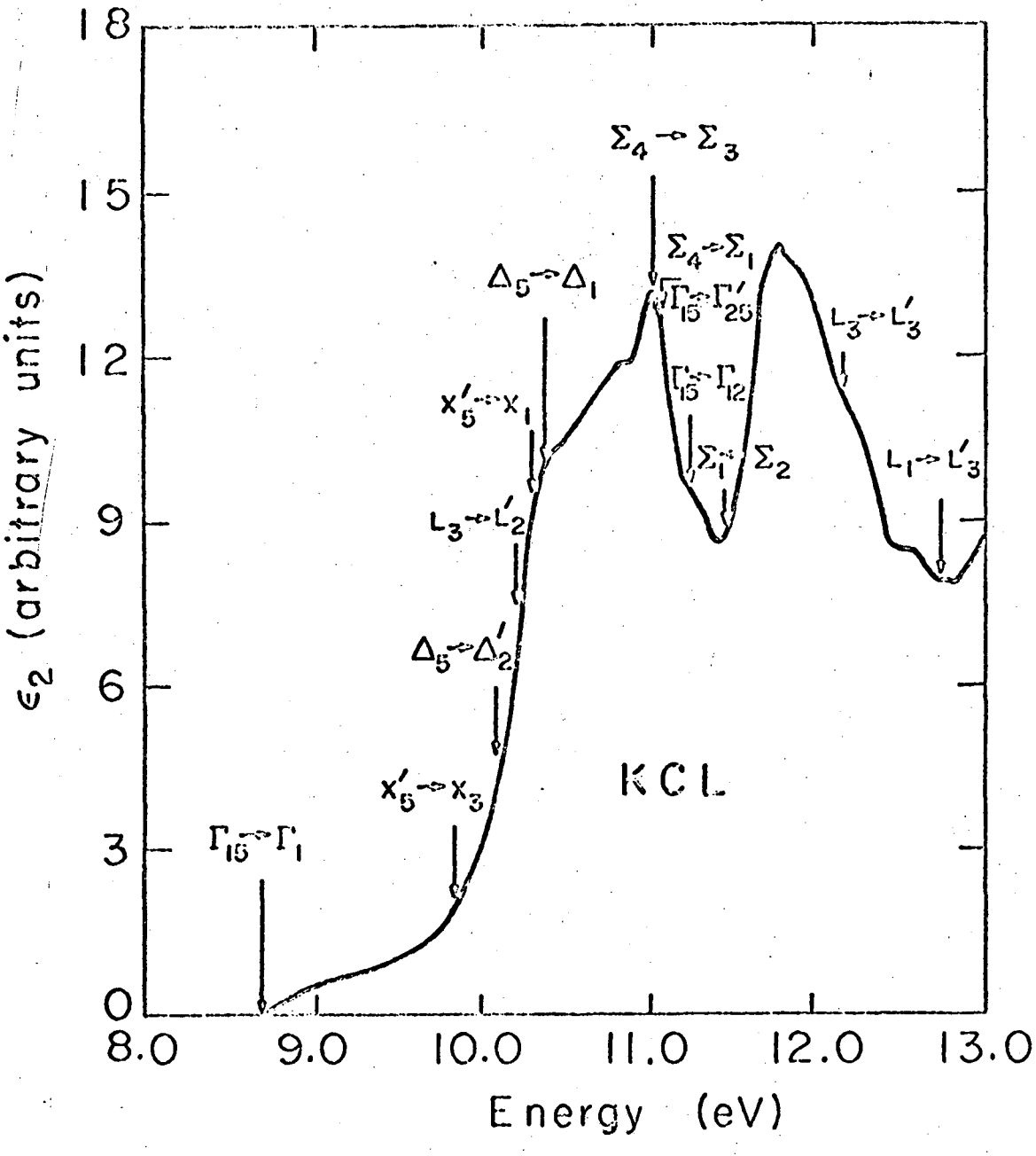

XBL6812-7326

Fig 15

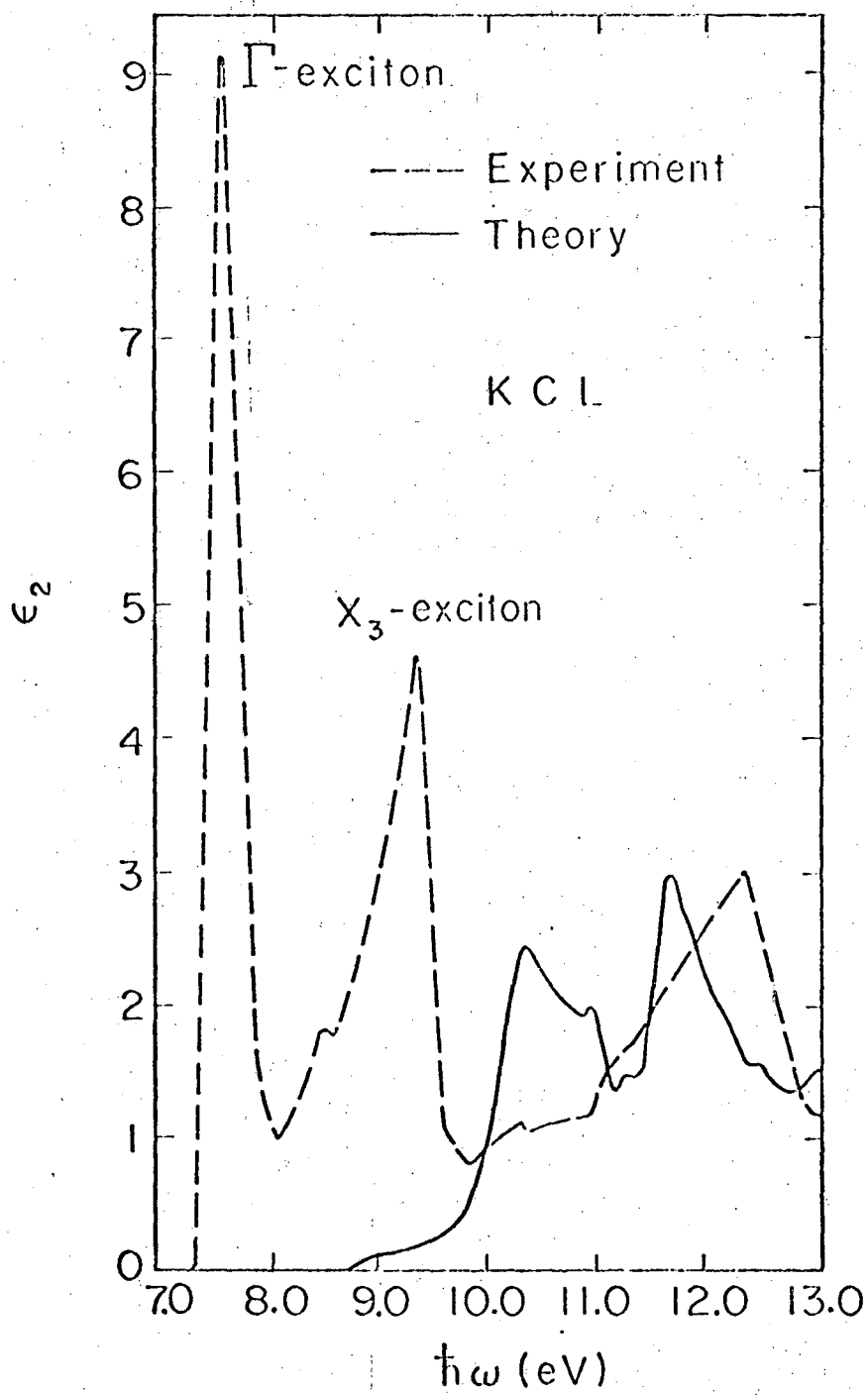

XBLG812-7327

Fig 16

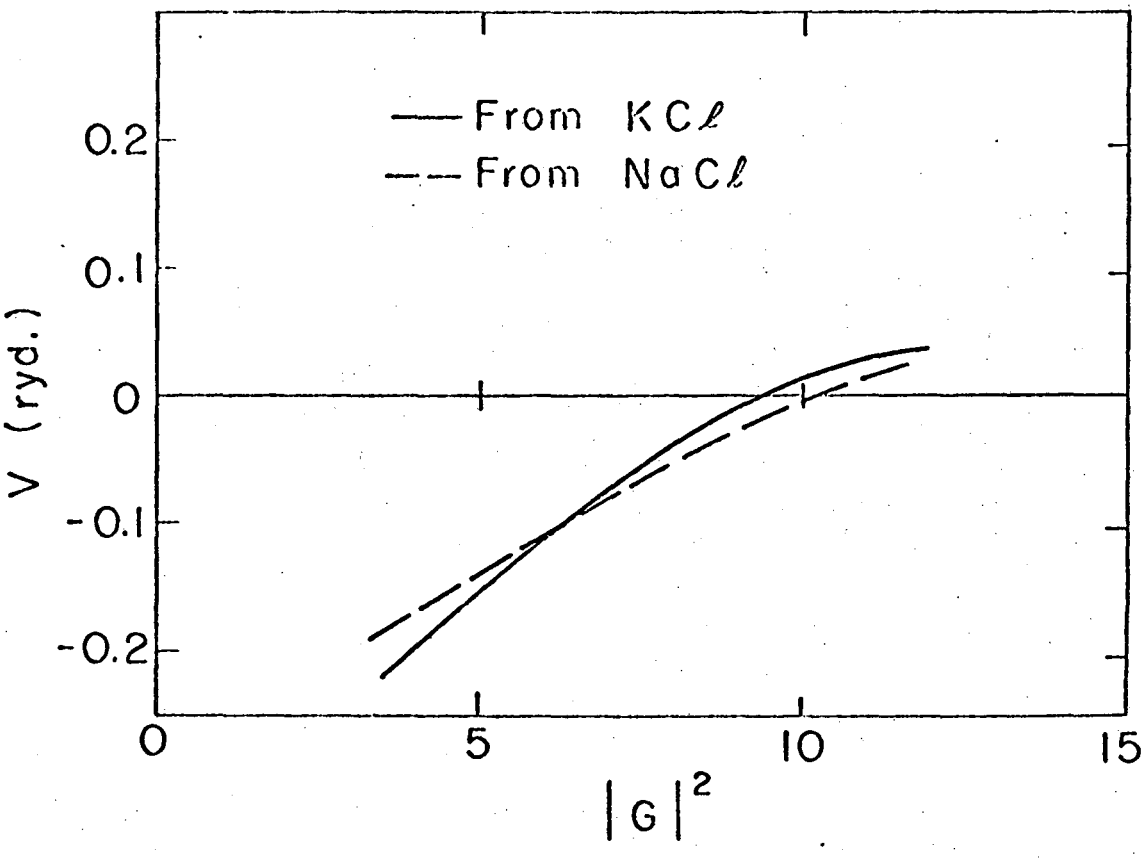

XBL6812-7329

Fig. 11

TECHNICAL INFORMATION DIVISION
LAWRENCE RADIATION LABORATORY
UNIVERSITY OF CALIFORNIA
BERKELEY, CALIFORNIA 94720